

Short-range order and clustering kinetics in a nondilute ternary alloy

Chantal K. Sudbrack,^{1,*} Ronald D. Noebe,² and David N. Seidman^{1,†}¹ Department of Materials Science and Engineering,
Northwestern University, Evanston, IL 60208 USA² NASA Glenn Research Center, Cleveland, OH 44135 USA

(Dated: December 22, 2018)

Solute-centered radial distribution functions, evaluating clustering and short-range order (SRO) in atom-probe tomographic images, characterize the kinetic pathways during the early-stage decomposition ($t \leq 600$ s) in a Ni-5.2 Al-14.2 Cr at.% superalloy at 873 K. A distribution of Cr-depleted Ni₃Al-SRO domains, $\langle R \rangle \cong 0.6$ nm, results from Al diffusion during quenching. Cr trapped in the domains exhibits a strong Al site-preference at $t=120$ s as the domain number density increases. With time, Al substitutes for trapped Cr leading to the initiation of $\gamma(\text{fcc})/\gamma'(\text{L1}_2)$ phase separation between 300-600 s.

PACS numbers: 64.75.+g, 81.30.Hd, 68.37.Vj, 61.18.-j

The interest in short-range ordering (SRO) and clustering processes, in the liquid and solid states, is strong and pervasive [1]. These processes have been primarily characterized in binary systems with small-angle scattering techniques in reciprocal lattice space [2, 3, 4], as meaningful quantification is difficult for multicomponent alloys. For substitutional ternary systems, the scattering intensity depends on three linearly independent pair correlation functions with three related partial structure functions [5], and requires that the partial structure functions be known for data deconvolution. In contrast to scattering methods, atom-probe tomography (APT) allows sub-nanometer chemical characterization in direct lattice space via the atom-by-atom reconstruction of a small volume, typically 10^4 nm^3 for a conventional APT. In a nondilute ternary system, SRO and clustering are evaluated in APT images with a radial distribution function (RDF) analysis. The Ni-5.2 Al-14.2 Cr at.% solid-solution, γ (fcc), contains low to moderate solute supersaturations at 873 K [6], and when aged isothermally, Ni₃(Al_xCr_{1-x}) precipitates, γ' (L1₂), form via a first-order phase transformation.

Cast ingots are homogenized at 1573 K for 24 h and 1123 K for 3 h; quenched sections are aged at 873 K (120 s–1024 h), and then electropolished to produce sharply-pointed needle-shaped specimens for APT experiments [6]. Spheroidal γ' -precipitates are first detected within APT images after 600 s of aging with 9 at.% Al isoconcentration surface analyses, which identify precipitates as small as 0.45 nm in radius (R), 20 detected atoms [6]. Between 600 and 900 s, the γ' -number density increases sharply ($5.9 \pm 1.7 \cdot 10^{21} \text{ m}^{-3} \text{ s}^{-1}$) with a constant $\langle R \rangle$ (0.75 nm) [6], consistent with steady-state nucleation behavior. In Fig. 1, a $12 \times 5 \times 2 \text{ nm}^3$ slice from an APT analysis along a [001]-direction displays a γ' -precipitate, $R=0.8$ nm, from a specimen aged for 600 s, where the γ/γ' interface is delineated with a 9 at.% Al surface. The precipitate's Al-rich {200} L1₂-superlattice planes ($2d_{200}=0.356$ nm) are clearly resolved. The solute

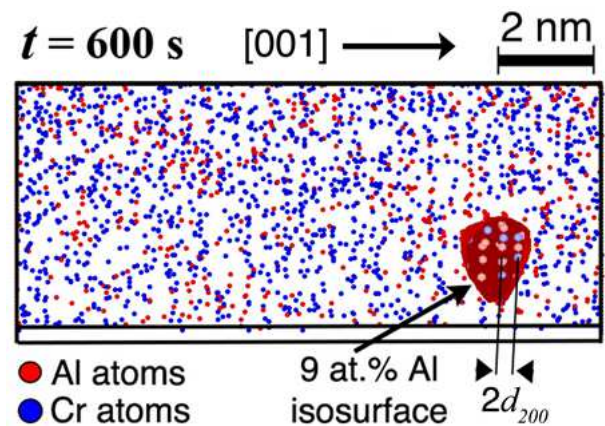


FIG. 1: Within Ni-5.2 Al-14.2 Cr at.% APT reconstructed volumes, Al-rich γ' -precipitates are delineated with 9 at.% Al isoconcentration surfaces and are first detected after aging for 600 s at 873 K [6]. The Al and Cr atoms in this $12 \times 5 \times 2 \text{ nm}^3$ slice, displayed in red and blue, are enlarged in the γ' -precipitate ($R=0.8$ nm) to emphasize the resolved {002} superlattice planes perpendicular to the [001] analysis direction.

distributions in Fig. 1 provide direct visual evidence for phase separation and demonstrates that atoms are positioned with sub-nanometer resolution. Short-range processes operating prior to the observed precipitation ($t \leq 600$ s) are not suitably addressed with the isoconcentration analyses, thus an RDF analysis that provides spatial sensitivity and resolves lattice site-specific information is introduced.

An RDF at a given radial distance, r , is defined as the average concentration distribution of component i around a given solute species, X, $\langle C_i^X(r) \rangle$, normalized to the overall concentration of i atoms, C_i^o , in the sampled volume:

$$RDF = \frac{\langle C_i^X(r) \rangle}{C_i^o} = \frac{1}{C_i^o} \sum_{k=1}^{N_X} \frac{N_i^k(r)}{N_{TOT}^k(r)}; \quad (1)$$

where $N_i^k(r)$ is the number of i atoms in a radial shell about the k^{th} X atom and centered at r , $N_{TOT}^k(r)$ is the total number of atoms within this shell, and N_X is the total number of X atoms in the sampled volume. The average concentration distributions around a solute species in 0.01 nm thick shells are smoothed with a weighted moving average using a Gaussian-like spline function [7], with a 0.05 nm full-width half-maximum, where $\langle N_{TOT}(r) \rangle$ increases quadratically with r . Only the RDFs for $r \geq 0.2$ nm are presented as the physical interpretation at smaller r is difficult due to possible ion trajectory effects. An RDF value of unity is characteristic of a perfectly random distribution, while values that differ describe clustering or ordering tendencies. The absolute magnitude of these processes can be compared with the RDF's amplitude, $A=[\text{RDF}(r)-1]$. An RDF value > 1 indicates a greater concentration than the overall concentration (positive correlation), while a value < 1 implies a smaller one (negative correlation).

An RDF's shape and magnitude when analyzing APT data is first evaluated for a well-defined system, a nearly-pure [8] Ni_3Al (L1_2) alloy [9], and compared to the expected values for a theoretical Ni_3Al alloy, exhibiting perfect long-range order (LRO) (Fig 2). In the theoretical alloy, Eq. 1 yields RDF values for the Al-Al profile that alternate discretely as a series of delta-functions between 0 and 4 at successive nearest neighbor (NN) distances (vertical lines in Fig 2), while the Al-Ni values alternate between $4/3$ and 0 (not displayed). Due to mass conservation, one RDF is sufficient to describe the LRO behavior in a binary alloy; therefore, only the Al-Al profiles are compared, where the random-state, $\text{RDF}=1$, is denoted by a horizontal dashed line. Compared to the theoretical profile (*right* ordinate), the experimental profile (*left* ordinate) is damped (ca. 9 times smaller in A than the theoretical value at the 1st NN distance) and does not alternate strictly between positive and negative correlation, a result of the uncertainty in atomic positioning. The measured intensities of the Al-Al and Al-Ni RDFs are stronger at the 1st NN distance than at longer distances. These RDFs oscillate over the full range of r , $r \leq 1$ nm, a defining characteristic of LRO. The observed shape results from contributions of adjacent NNs to the measured concentrations and is a function of the number of NNs (parenthetical values in Fig. 2) and their weighted contribution (proportional to theoretical A values). The disparity with theory is understood by considering the value for a particular NN. The RDF, Eq. 1, is not normalized to the coordination number, Z , as Z assignment is somewhat ambiguous; hence, a greater number of NNs contribute more to the measured RDF than fewer with the same A . At the 3rd NN distance, although theory predicts a negative correlation, the observed positive correlation results from the positive contributions from the six adjacent 2nd NNs and 12 4th NNs, each with larger weighting factor ($A=3$) than the 24 3rd NNs ($A=-1$). If

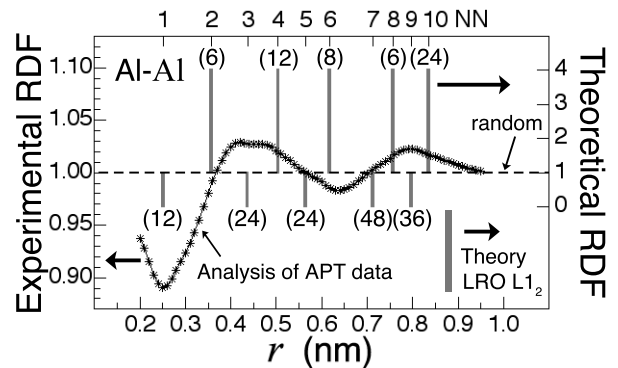


FIG. 2: Al-Al RDFs (Eq. 1) vs. radial distance, r , out to the 10th nearest neighbor (NN) distance for a near stoichiometric Ni_3Al (L1_2) alloy [8] analyzed by APT and a theoretical alloy assuming perfect LRO. The number of L1_2 NNs at corresponding distances is indicated in parentheses. $\text{RDF}=1$ (random solid solution) is indicated by a dashed line.

the distributions of reconstructed atom positions about each NN distance are known, it would be possible to obtain a deconvoluted RDF, allowing pair interaction energies to be determined.

Figure 3 presents experimentally determined Al- and Cr-centered RDFs for the as-quenched (AQ) state and after 120 s of aging. In the AQ specimen (open circles), the Al-Al and Al-Ni RDFs deviate from the random state (dashed horizontal line), where the deviations are comparable to the ones for the LRO alloy (Fig 2); unlike the LRO alloy, however, they occur over a short-range, $r \leq 0.6$ nm. At the 1st NN distance, the Al-Al and Al-Ni correlations are negative and positive, respectively, and the Al-Al RDF's oscillations are coupled with oscillations in the Al-Ni RDF that are opposite in sign, consistent with L1_2 ordering. These trends establish the presence of quenched-in L1_2 SRO domains with $\langle R \rangle \cong 0.6$ nm. After 120 s (solid diamonds), the SRO in the fcc solution (matrix) increases as indicated by the larger Al-Al and Al-Ni RDFs' intensities. The RDFs' deviations also extend 0.6 nm; thus, the average size of SRO domains remains ca. constant with aging to 120 s as the number density increases concomitantly. As solute concentrations are not in the dilute limit, the volumes are reasonably well-sampled, yielding Al-Cr and Cr-Al profiles that are nearly similar. These RDFs sustain a negative spatial correlation over the distances analyzed, $r < 1$ nm, establishing that the γ' -SRO regions are Cr depleted and the initial quench rate is insufficient to avoid diffusion of Al away from Cr, as Al diffuses faster than Cr in Ni-Al-Cr. In conjunction with more developed SRO at 120 s, the intensity of the Al-Cr RDF at the 1st NN distance is strongly negative, which suggests that Cr atoms do *not* prefer to be NNs to Al and they occupy the Al sites within the $\text{Ni}_3(\text{Al,Cr})$ -type SRO domains. In the AQ state, Cr is completely randomly distributed relative

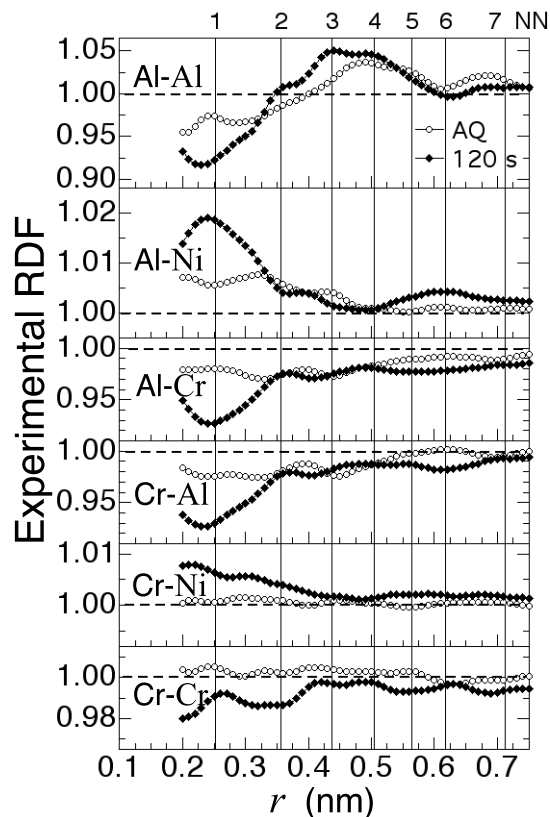


FIG. 3: RDF vs. radial distance, r , out to the 7th NN distance for as-quenched (AQ) Ni-5.2 Al-14.2 Cr at.% and after aging for 120 s at 873 K. The negative and positive correlations at the 1st NN in the Al-Al and Al-Ni profiles establish L1₂-order.

to other Cr and Ni atoms as indicated by the flat Cr-Cr and Cr-Ni RDFs, consistent with Cr's smaller diffusivity. After 120 s, these RDFs deviate from random, and at the 1st NN distance, exhibit positive Ni and negative Cr correlations, supporting a possible Ni-Cr ordering tendency either within Al-rich domains or matrix.

Since the RDF is applied to total volumes, as phase separation progresses the RDF becomes a convolution of the SRO and clustering processes in both phases. Large fluctuations in concentration yield cumulative shifts in the RDF away from unity (Eq. 1). Figure 4 presents the RDF analysis for 120, 300, and 600 s. With aging, the Al-Al RDF exhibits a cumulative shift towards higher values, slight at 300 s (open squares) and strong at 600 s (open circles with a central point), consistent with the γ' -phase detection with isoconcentration surfaces at 600 s [6] (Fig. 1); thus, phase separation occurs *after* SRO establishment. This strong Al-Al shift, however, is not accompanied by strong shifts in the Cr-Cr RDFs. Overall, the Cr-Cr RDF has a *slight* negative correlation at 120 s (solid diamonds), which may result from Cr ordering in the domains, and exhibits a gradual shift in the positive direction with aging. Cr clearly partitions to γ more slowly than Al to γ' . After 120 s, the Al-

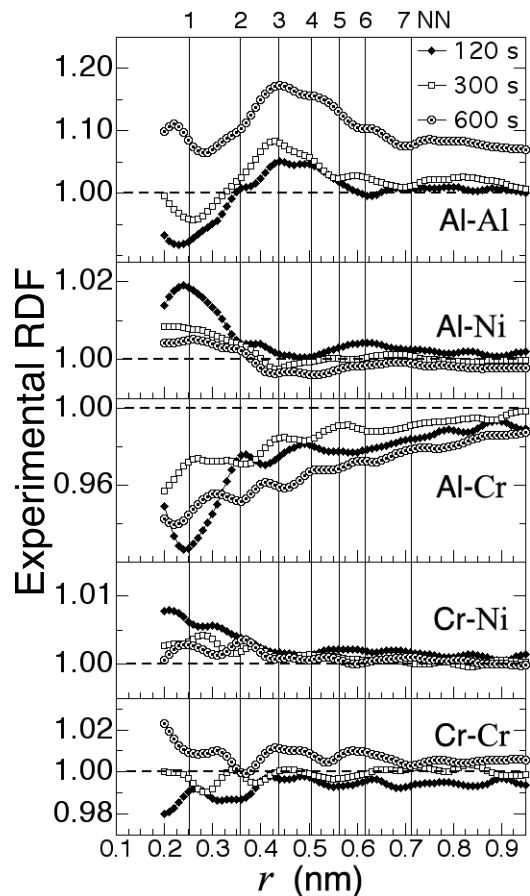


FIG. 4: RDF vs. radial distance, r , for Ni-5.2 Al-14.2 Cr at.% aged for 120, 300, or 600 s at 873 K. The overall Al-Al shift to higher RDF values after 300 s demonstrates that the onset of γ' -phase separation occurs between 300 and 600 s.

Cr RDF exhibits a strong negative correlation at the 1st NN distance that becomes less intense after 300 s, while at longer distances the RDFs' intensities are comparable. This trend is attributed to the substitution of Al for Cr in the SRO domains after 300 s leading to less retained Cr. As the alloy is aged from 300 to 600 s, the Al-Cr RDF retains its shape; however, a cumulative shift in the negative direction is observed as the alloy phase separates. The Al-Ni RDF after 120 s exhibits an ordering tendency at the 1st NN distance that damps toward unity with aging, which establishes that the overall L1₂-ordering in $\gamma+\gamma'$ phases diminishes. At 600 s, the γ' -phase forms with a vol. fraction of 0.11 ± 0.04 and γ' -LRO is established at a high Al concentration (19.1 ± 1.7) [6]; thus, ordering increases locally within γ' . The damping trend reflects the diminishment of SRO in γ , while processes in γ contribute more strongly to the measured RDF than those in γ' .

The possible early-stage kinetic pathways of a first-order phase transformation that involve ordering, such as fcc \rightarrow L1₂, have been evaluated by mean-field thermo-

dynamic models [10, 11], which predict that low supersaturation systems proceed via nucleation and growth of the ordered phase. While higher supersaturation systems heterogeneously order congruently prior to phase separation, and systems within the spinodal, continuously order. For a nearly identical alloy, Ni-5.2 Al-14.8 Cr at.%, also aged isothermally at 873 K, LKMC simulations [12] indicate that phase separation occurs by nucleation and growth, which is preceded by two stages: first, a Ni₃Cr-type (DO₂₃) SRO phase, followed by the development of L1₂-type SRO. This behavior is *not* observed experimentally. RDFs establish L1₂-type SRO in the AQ state that becomes stronger after 120 s of aging (Fig. 3). The distribution of Cr and Ni atoms relative to Cr atoms is completely random in the AQ alloy, hence Ni₃Cr-type SRO *does not* precede the L1₂-type SRO. A slight Cr-Ni ordering tendency is observed after 120 s, thus Ni₃Cr-type SRO may be established *after* L1₂-type SRO. The onset of Al-rich γ -phase separation (Fig. 4) is shown to occur *after* 300 s of aging after SRO development.

A crucial difference between our experiments and the LKMC simulation [12] is the thermal history of the AQ state. In the LKMC simulation the initial state is a random distribution of atoms, thereby neglecting the influence of a finite quench rate from 1123 K to room temperature, followed by up-quenching to 873 K. The influence of the quench rate is twofold. Firstly, it leads to a supersaturation of quenched-in vacancies, and, secondly, phase separation may occur, particularly in alloys with a large solute supersaturation and/or small interfacial free-energy, where the nucleation barriers are small and nucleation currents large [13]. The half-life of excess vacancies for diffusion-limited annihilation at dislocations is $\tau_{1/2} = 0.693 \ln(R_d/r_c) / 2\pi N_d D_{1v}$ [14], where N_d is the dislocation density (ca. 10^{10} m^{-2} to 10^{12} m^{-2}), R_d is the distance between dislocations, $(\pi N_d)^{-1/2}$, r_c the dislocation core radius (ca. one Burgers vector, 0.255 nm for γ -phase). The monovacancy diffusivity is $D_{1v} = a^2 \nu f_{1v} \exp(s_{1v}^n/k_B) \exp(-h_{1v}^n/k_B T)$, where a is the lattice parameter, $a^\gamma = 3.552 \times 10^{-10} \text{ m}$ [6], f_{1v} is the correlation factor for a monovacancy diffusion mechanism, 0.781, ν is the Debye frequency for Ni, $9.38 \times 10^{12} \text{ s}^{-1}$, s_{1v}^n is entropy of migration for a monovacancy ($\sim 0.5k_B$), and h_{1v}^n is the monovacancy migration enthalpy in Ni, 1.30 eV [15]; therefore, D_{1v} is $4.77 \times 10^{-14} \text{ m}^2 \text{ s}^{-1}$ at 873 K. For $N_d = 10^{10} \text{ m}^{-2}$, $\tau_{1/2} = 7902 \text{ s}$, while $N_d = 10^{12} \text{ m}^{-2}$ implies $\tau_{1/2} = 84 \text{ s}$, which are lower bounds for $\tau_{1/2}$ since dislocation climb is assumed to be diffusion-limited [16]. Suggesting that quenched-in excess vacancies play a significant role in the early-stages of decomposition.

In summary, the local environment around solute atoms in a nondilute Ni-Al-Cr alloy, as it evolves temporally, is determined from direct-space APT images, Fig. 1, using RDFs (Eq. 1); thereby providing a new methodology to test an alloy's homogeneity and investigate SRO. As seen by comparing the measured RDF

with the expected RDF for a fully ordered Ni₃Al (L1₂) alloy, Fig. 2, the APTs positional uncertainty leads to a significantly damped profile that is sensitive to the evaluation of both site-preference and the spatial extension of ordering. Phase separation is preceded by Ni₃(Al,Cr) SRO (L1₂), which extends spatially to ca. 0.6 nm, Fig. 3, and is present in the AQ alloy due to its thermal history, with decomposition being assisted by quenched-in vacancies. Relative to the solid solution, the Ni₃(Al,Cr) SRO domains are depleted in Cr, and as the alloy evolves temporally, Al is found to substitute for Cr within the Ni₃(Al,Cr) SRO domains. A strong cumulative shift in the Al-Al RDF establishes that the onset of phase separation occurs between 300 and 600 s (Fig. 4), while the γ -matrix SRO diminishes with the decay of Al-Ni ordering during phase separation.

This research is sponsored by the National Science Foundation, grant DMR-0241928; CKS received partial support from an NSF graduate fellowship. We thank Dr. Z. Mao and Prof. M. Asta for helpful discussions.

* Electronic address: csudbrack@alumni.reed.edu

† Electronic address: d-seidman@northwestern.edu

- [1] J. M. Ziman, *Models of Disorder* (Cambridge University Press, Cambridge, 1979).
- [2] G. Kostorz, in *Physical Metallurgy*, edited by R. W. Cahn and P. Haasen (Elsevier Science BV, Amsterdam, 1996) 4th Ed., p. 1116.
- [3] B. Schönfeld, *Prog. Mater. Sci.* **44**, 435 (1999).
- [4] H. Reichert *et al.*, *Phys. Rev. Lett.* **87** 236105 (2001).
- [5] D. de Fontaine, *J. Appl. Cryst.* **4**, 15 (1971); *J. Phys. Chem. Solids* **34**, 1285 (1973).
- [6] C. K. Sudbrack, Ph.D. thesis, Northwestern University (2004). <http://www.at.northwestern.edu/etd>
- [7] O. C. Hellman *et al.*, *Microsc. Microanal.* **6**, 437 (2000).
- [8] This APT volume contains 295,705 atoms, including trace amounts of Ta, Cr and B, where the measured composition of the Ni₃Al lattice is $C_{Ni} = 73.93 \pm 0.16$, $C_{Al} = 25.29 \pm 0.16$, $C_{Ta} = 0.51 \pm 0.03$, and $C_{Cr} = 0.27 \pm 0.02$ at.%, with 456 B atoms occupying interstitial sites [6].
- [9] G. P. E. M. van Bakel, K. Hariharan and D. N. Seidman *Appl. Surf. Sci.* **90**, 95 (1995).
- [10] A. G. Khachaturyan, T. F. Lindsey, and J. W. Morris, *Metall. Trans. A* **19**, 249 (1988).
- [11] W. A. Soffa and D. E. Laughlin, *Acta Metall.* **37**, 3019 (1989).
- [12] C. Pareige *et al.*, *Acta Mater.* **47**, 1889 (1999).
- [13] G. Martin, in *Solid State Phase Transformation in Metals and Alloys: Ecole d'été d'Aussois, 3-15 septembre 1978* (Les Éditions de Physique, Orsay, 1980) p. 337.
- [14] D. N. Seidman and R. W. Balluffi, *Phys. Stat. Sol.* **17**, 531 (1966).
- [15] L. C. Smedskjaer *et al.*, *J Phys. F: Metal Phys.* **11**, 2221 (1981)
- [16] D. N. Seidman and R. W. Balluffi, in *Lattice Defects and Their Interactions*, edited by R. R. Hasiguti (Gordon and Breach Science Publishers, New York, 1967) p. 911.